Supplementary Information

Crack growth-driven wettability transition on carbon black /polybutadiene nanocomposite coating via stretching

Meng Ren[a], Xin Hu[b], Yongsheng Li[a], Hong Shao[a], Peng Jiang[c], Wenwen Zeng[a], Cong Wang[a], and Changyu Tang[a]*

a. Chengdu Green Energy and Green Manufacturing Technology R&D Center, Chengdu Development Center of Science and Technology, China Academy of Engineering Physics, Chengdu, 610200, China.

b. Chemical and Biological Engineering (CBE), Hong Kong University of Science and Technology, Hong Kong, 999077, China.

c. Leshan Shizhong District Environmental Monitoring Station, No. 2000 Changqing Road, Shizhong District, Leshan City, 614000, China.

* Address correspondence to:

Changyu Tang: sugarchangyu@163.com
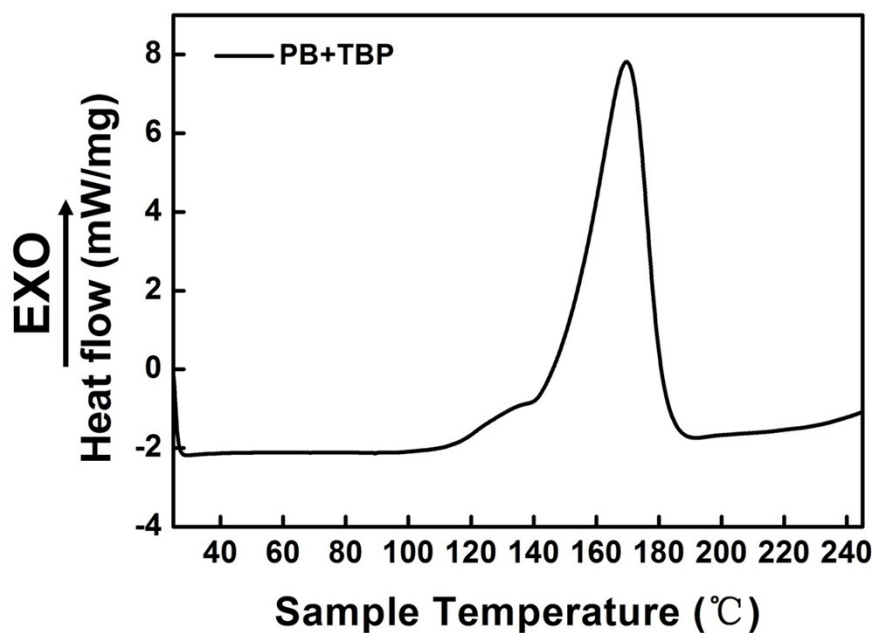
Figure S1. DSC curve of PB containing 4% TBPB scanned from 25 to 240 °C.
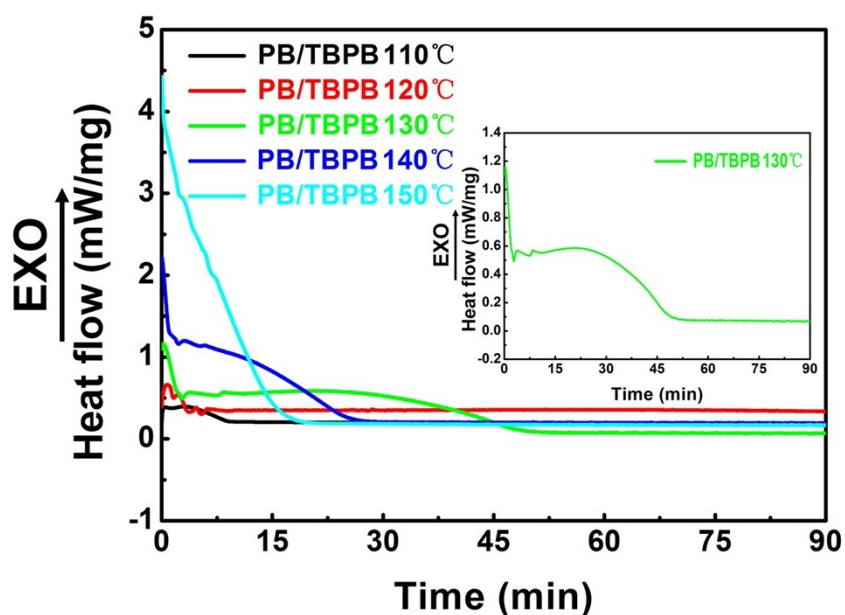
Figure S2. DSC curves of PB containing 4% TBPB cured at different temperatures.

With the help of thermal initiator (TBPB), PB cross-linking reaction begins at ~110 °C and reaches the maximum reaction rate at ~170 °C. The curing temperature should be more than 110 °C. However, the rubber substrate under coating is easily aged at

curing temperature over 130°C. Thus, the curing temperature at 130 °C is selected.
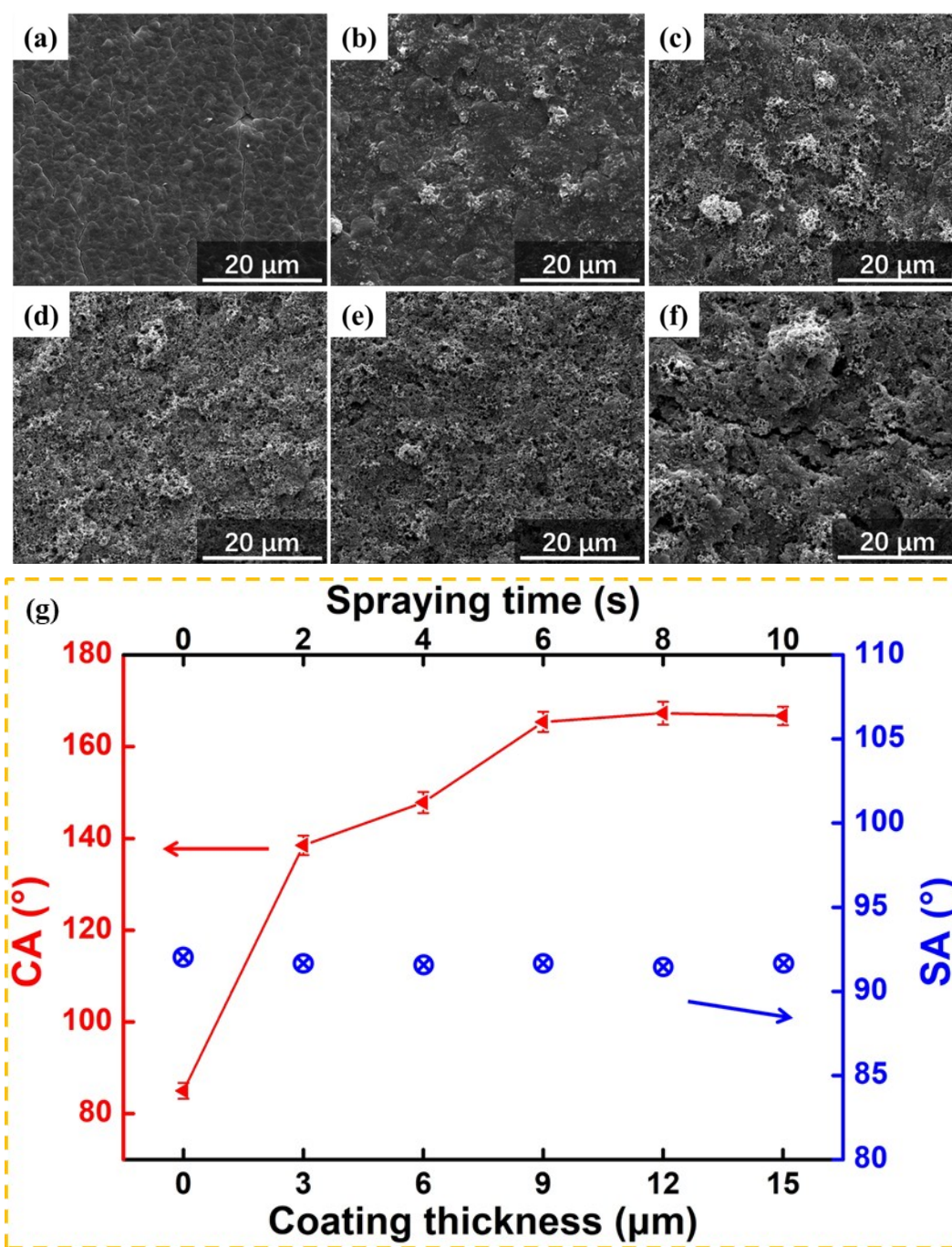
Figure S3. SEM morphologies of 1:15 CB/PB prepared with various spraying time: (a) 0 s, (b) 2 s, (c) 4 s, (d) 6 s, (e) 8 s, and (f) 10 s; (g) shows CAs and SAs of composite coatings with various coating thickness and corresponding spraying time.

⊗ indicates that water droplet cannot slide on the coating due to so large SA.

Generally, spraying time affects the surface morphology of superhydrophobic coatings. Scanning electron microscopy (SEM) is employed to observe the surface morphology change of the composite coating as a function of the spraying time. Here, the CB/PB mass ratio of is kept at 1:15. With increasing spraying time, the thickness and roughness of the coating on the rubber substrate increased and the resultant coating was transformed into Wenzel superhydrophobic state at spraying time of 8 s. Further increasing the spraying time led to low mechanical strength and poor uniformity.
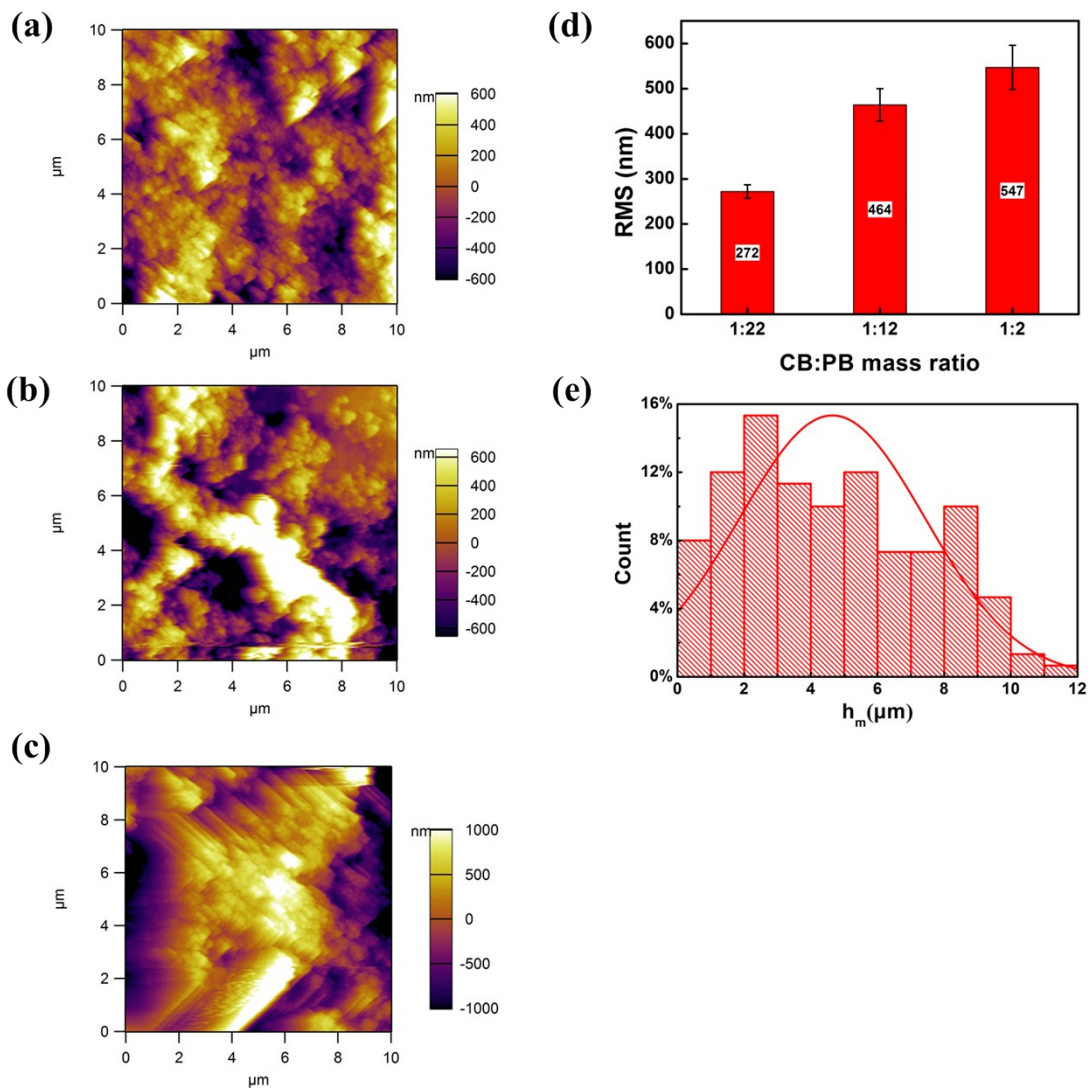
Figure S4. AFM images of CB/PB composite coating with mass ratios of (a) 1:22, (b) 1:12, and (c) 1:2. The histogram obtained from SEM statistical data (d) showing the height of micro-scale mastoids in CB/PB coating with mass ratios over 1:12.

Before stretching ➡ After stretching
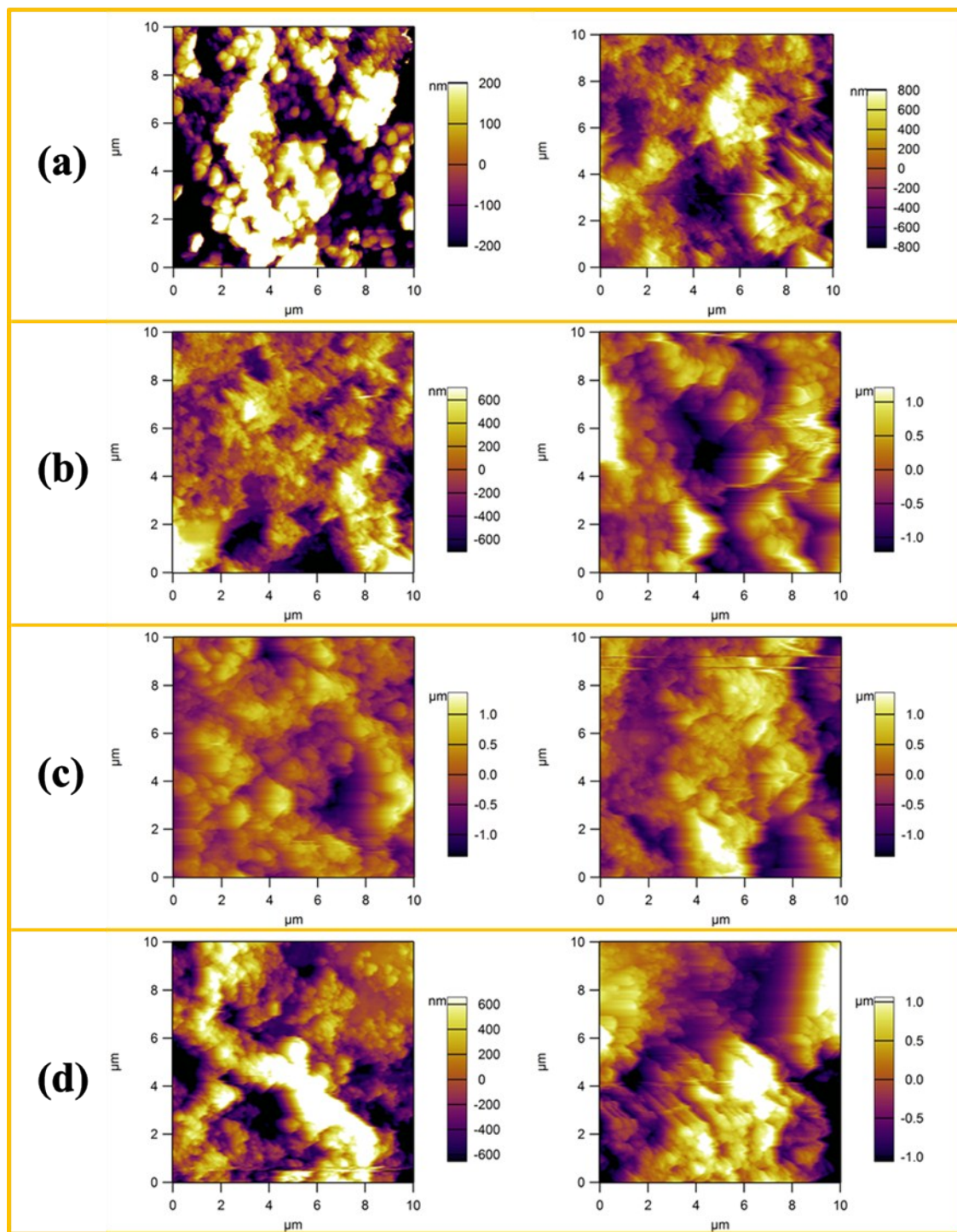
Figure S5. AFM of CB/PB composite coating before and after stretching: (a) CB/PB=1:20, (b) CB/PB=1:18, (c) CB/PB =1:15, and (d) CB/PB =1:12.
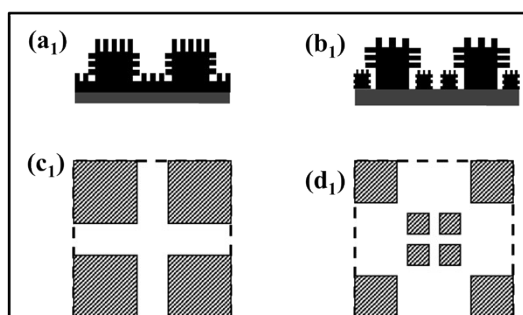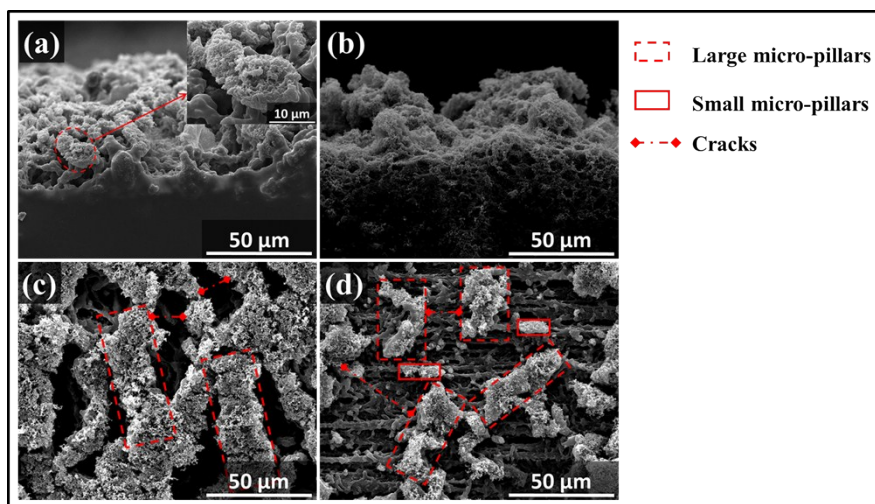
Figure S6. SEM images of CB/PB coating stretched to various strains: (a) and (b) are the side views at low strain and high strain, respectively; (c) and (d) are the corresponding front views. According to the SEM images, the model can be illustrated in Figure (a_1-d_1).
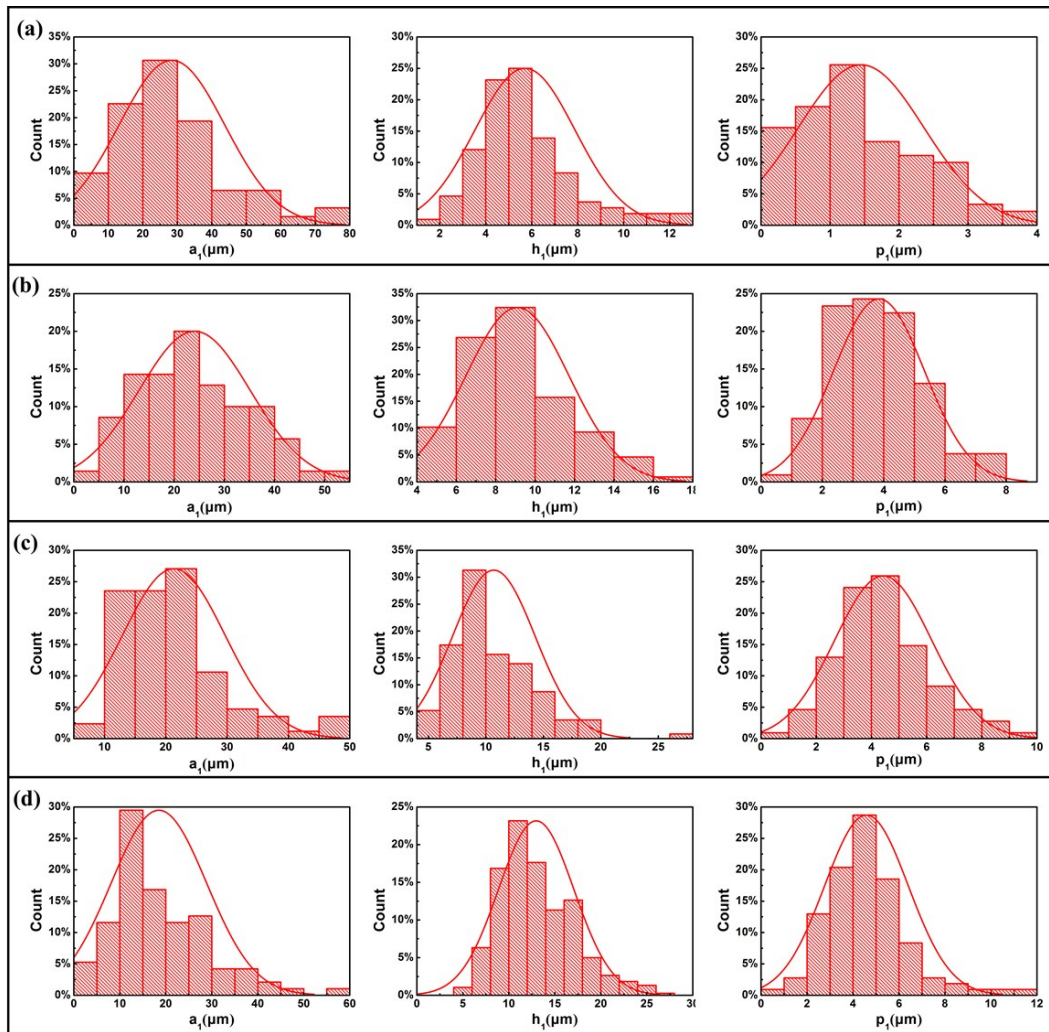
Figure S7. Histograms showing the geometric parameters of roughness of CB/PB coatings with various mass ratios of (a) 1:20, (b) 1:18, (c) 1:15, and (d) 1:12 at low strain (~100-300%).
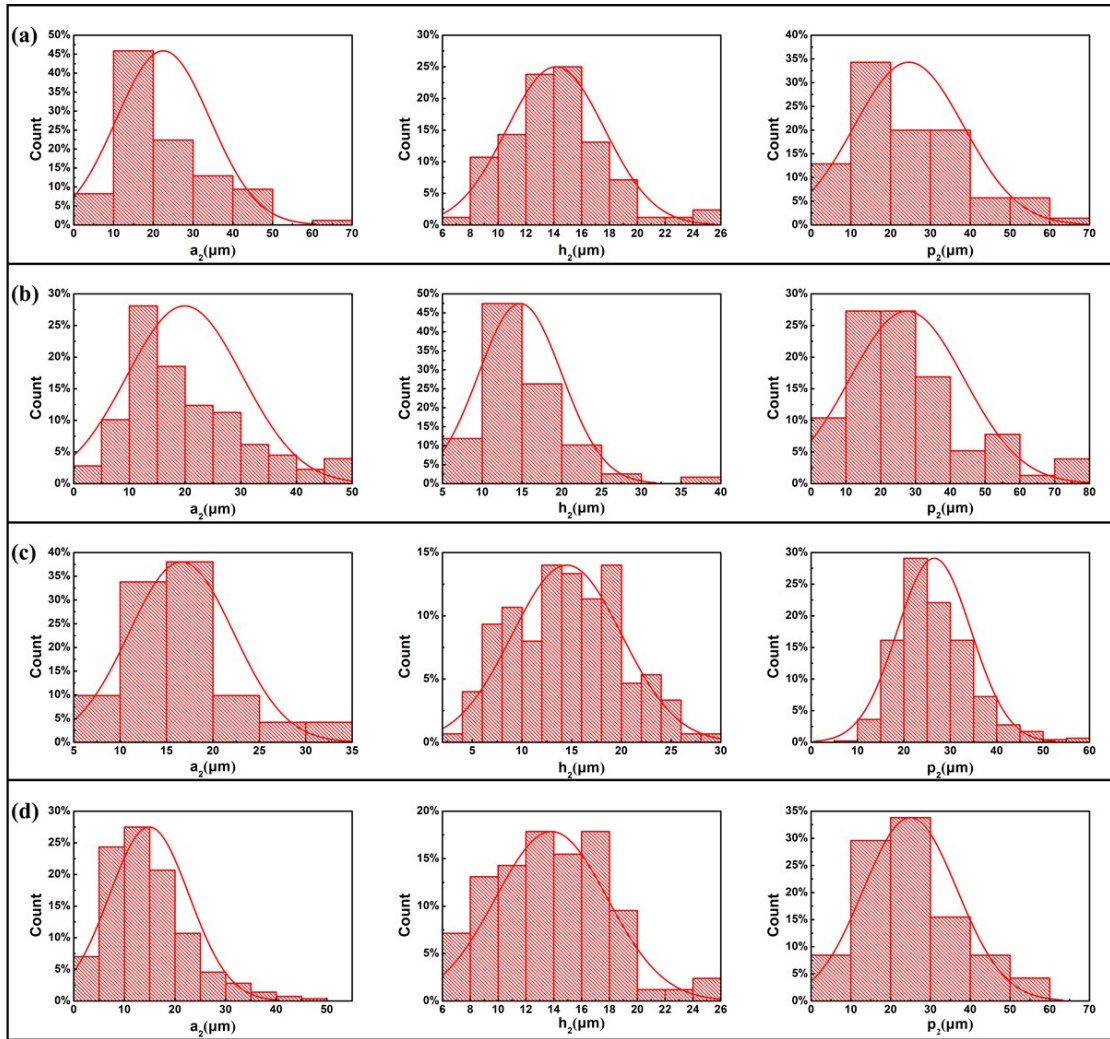
Figure S8. Histograms showing the geometric parameters of roughness of CB/PB coatings with various mass ratios of (a) 1:20, (b) 1:18, (c) 1:15, and (d) 1:12 at high strain (~400-800%).
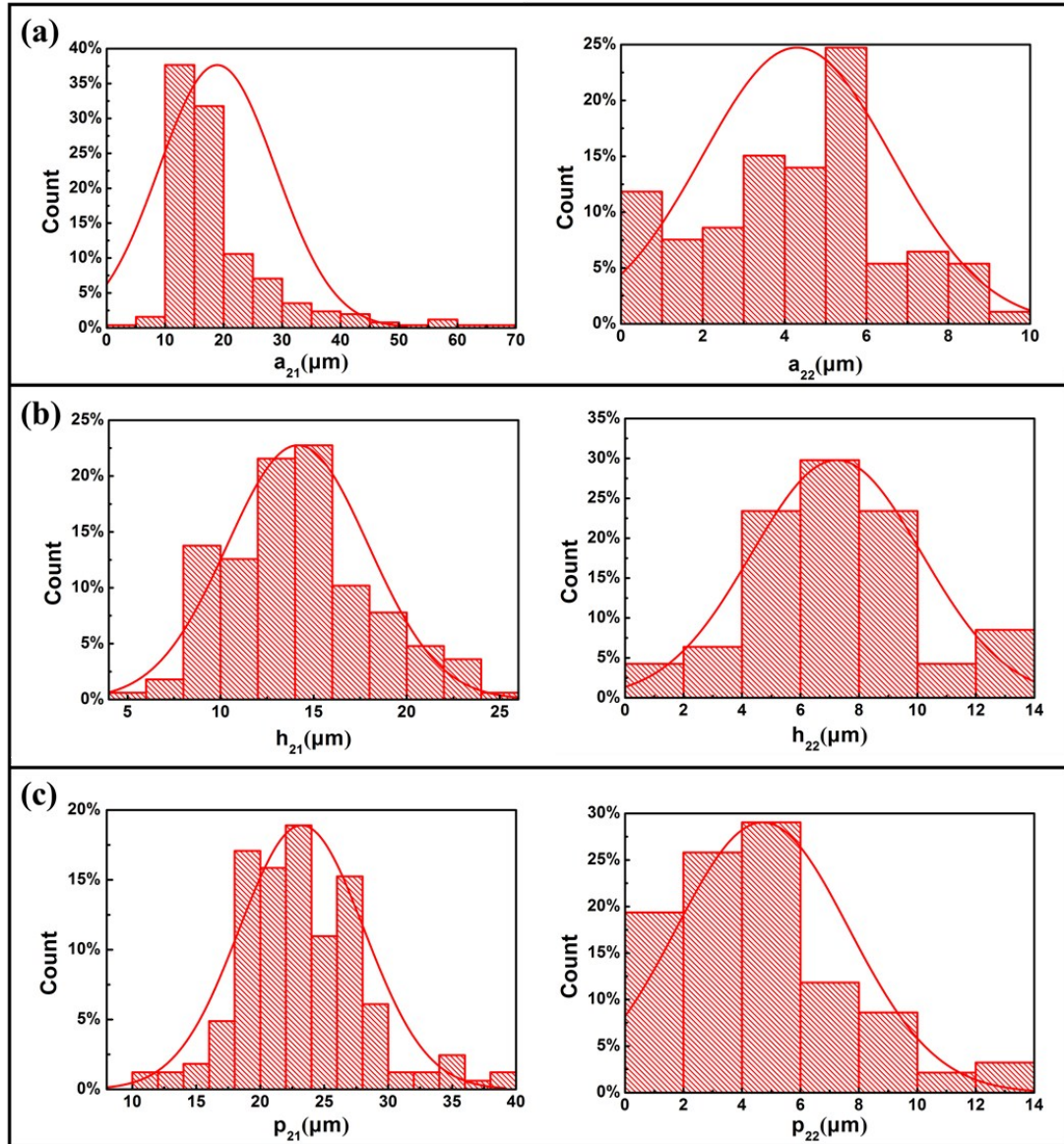
Figure S9. Histograms showing the geometric parameters relationship in Model II: (a) the side length of large rectangular pillars (a_{21}) and small rectangular pillars (a_{22}), (b) the height of large rectangular pillars (h_2) and small rectangular pillars (h_1), (c) the pitch distance of large rectangular pillars (p_{21}) and small rectangular pillars (p_{22}).

Modeling calculation and analysis
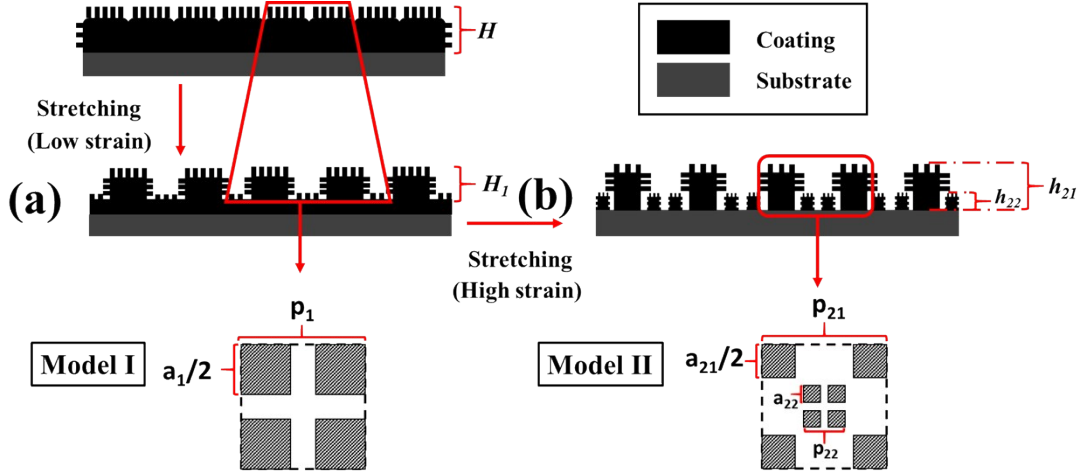
Figure S10. Effect of spatial distance and size on Wenzel-Cassie transition during stretching coating. Model I and Model II depict the change in roughness of composite coating at (a) low and high (b) stretching strain, respectively.

Model I and II represent the morphology changes in composite coatings at low and large strains. Combining SEM images, Wenzel, and Cassie models, the effects of geometric parameters on the wettability of composite coatings are quantitatively analyzed. In Wenzel model that describes water droplet wets the grooves of rough surface completely, the apparent contact angle of the droplet, θ_w is given by equation (S1). In Cassie model, the apparent angle of the droplet that suspends on the roughness peaks, θ_c is given by equation. (S2), as follows:

$$\cos\theta_w = r\cos\theta_f \tag{S1}$$

$$\cos\theta_c = -1 + f_s(1 + \cos\theta_f) \tag{S2}$$

Here, r represents the ratio of the actual area of liquid-solid contact to the projected area on the horizontal plane, f_s represents the fraction of the apparent liquid-solid contact. θ_f is the equilibrium contact angle of water on the flat surface

and was measured to be 100° (the hybrid coating was pressed into a pellet to measure the contact angle). We assumed that the rough surface of the CB/PB composite coatings were composed of rectangular pillars with side length a, height h, and pitch distance p.

The SEM results present two distinct deformation models during different stages of stretching. Model I: at relatively low stretching strain (~100-300%), stretch results in an increase in space distance between the micro-structures but the morphology does not change obviously. According to equations (S1) and (S2), the CAs of composite coatings in Model I can be given respectively as follows:

$$\cos\theta_w = \left(1 + \frac{4B_1}{a_1 / h_1}\right)\cos\theta_f \tag{S3}$$

$$\cos\theta_c = -1 + B_1\left(1 + \cos\theta_f\right) \tag{S4}$$

Where

$$B_1 = \frac{1}{\left(1 + p_1 / a_1\right)^2}$$

Model II: at relatively high stretching strain (~400-800%), the cracks further propagate to divide the coating into many new microscaled mastoids with two different sizes and thus result in significant change (both size and pitch distance) in geometric parameters of the micro-structure. Taking the size change from the newly generated micro-mastoids into consideration, the wetting behavior corresponding to the Model II could be described by equations (S5) and (S6):

$$\cos\theta_w = r_1 r_2 \cos\theta_f$$

$$= \left[1 + \frac{4h_{21}}{a_{21}(1 + p_{21}/a_{21})^2}\right]\left[1 + \frac{16h_{22}}{a_{22}(2 + p_{22}/a_{22})^2}\right] \quad (S5)$$

$$= \left(1 + \frac{4B_{21}}{a_{21}/h_{21}}\right)\left(1 + \frac{8B_{22}}{a_{21}/h_{21}}\right)\cos\theta_f$$

$$\cos\theta_c = -1 + f_{s_1}f_{s_2}(1 + \cos\theta_f)$$

$$= -1 + B_{21}B_{22}(1 + \cos\theta_f) \quad (S6)$$

where

$$B_{21} = \frac{1}{(1 + p_{21}/a_{21})^2}$$

$$B_{22} = \frac{1}{(1 + 0.4 p_{21}/a_{21})^2}$$

Here, a_{21} and a_{22} represent the two-side length of newly generated micro-mastoids. According to the SEM measurement (as shown in Figure S9), $a_{22} = 0.25a_{21}$, $h_{22} = 0.5h_{21}$, $p_{22} = 0.2p_{21}$.

It is universally known that whether water droplets can wet the solid surface depends on the thermodynamic properties of the surface associated with geometric parameters, under which the water droplets always have the local minimum in energy. The energy formula of water droplet of given volume in equilibrium can be expressed as a function of the contact angle θ by the following equation:

$$G = (1 - \cos\theta)^{2/3}(2 + \cos\theta)^{1/3}(9\pi)^{1/3}V^{2/3}\sigma_{lv} \quad (S7)$$

where θ can be either θ_w or θ_c, V is the volume of the water droplet, σ_{ls} is the liquid-vapor surface energy per unit area (or surface tension).

According to equation S7, it can be easily verified that the right-hand side is a monotonically increasing function of $\cos\theta$ in the range of [-1,0], when the solid

surface condition is determined. As a result, the wettability of liquid on solid surface depends on an equilibrium droplet shape with lower value $\cos\theta$.
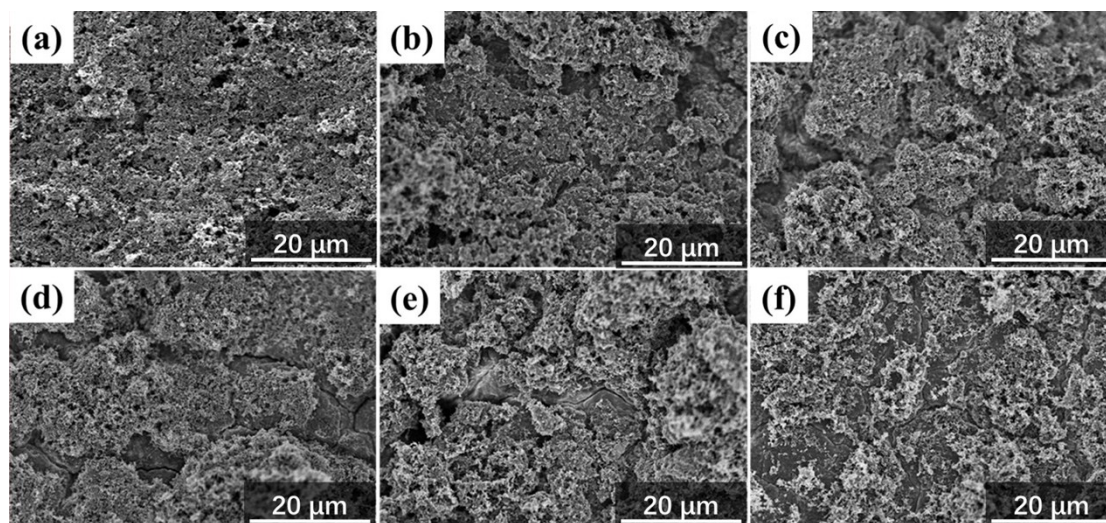
Figure S11. Surface SEM morphologies of coatings suffered from various stretching-releasing cycles: (a) 0, (b) 10, (c) 100, (d) 200, (e) 400, and (f) 1000.

Movie S1. Wenzel superhydrophobic coating captured a water droplet (6 μL) on Cassie superhydrophobic surface.

Movie S2. The attached droplet falls off the coating surface during stretching.